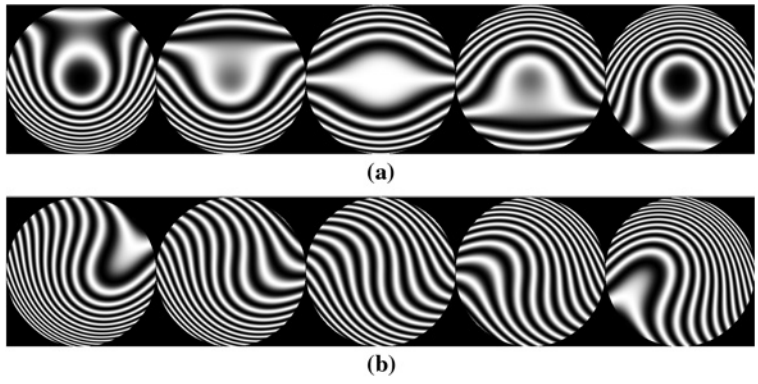

Figure 6.11 Vertical coma in the presence of defocus and tilt: (a) untilted and (b) tilted.

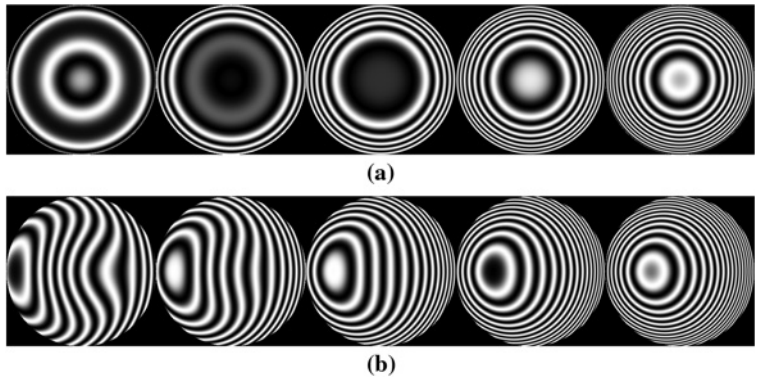

Figure 6.12 Spherical aberration in the presence of defocus and tilt: (a) untilted and (b) tilted.

6.7 Phase-Shifting Interferometry

6.7.1 Phase-shifting techniques

Phase-shifting interferometry is a powerful means of analyzing interferograms to recover the phase information. Traditionally, interferograms were measured by locating the center of a fringe and then tracing along the fringe. Phase-shifting interferometry avoids the need to track the location of the fringes and enables a point-by-point reconstruction of the wavefront. Consider a slightly modified version of Eq. (6.11), where

$$I(x, y; \phi) = I'(x, y) + I''(x, y)\cos[\Psi(x, y) + \phi]. \tag{6.23}$$

Here, $I'(x, y) = I_1 + I_2$, $I''(x, y) = 2\sqrt{I_1 I_2}$, and $\Psi(x, y) = (2\pi/\lambda)[W_1(x, y) - W_2(x, y)] + \phi_{12}$. In addition to the modified definition of the interference pattern, an extra factor ϕ has been added. Phase-shifting interferometry records multiple interferograms with different values of ϕ. In doing so, the phase $\Psi(x, y)$ at each point in the interferogram is easily

recovered. To control the value of ϕ, the interferometer is slightly adjusted between each measurement. This adjustment is typically performed by placing a piezo-electric transducer such as lead zirconate titanate (PZT) onto one of the mirrors in the interferometer. PZT is a ceramic that changes thickness in response to applied voltage. By applying specific voltages, small and precise movements of the mirror can be made. In the laser Fizeau and Twyman–Green interferometers, the reference surface is typically moved. In the Mach–Zehnder, the mirror in the reference arm is typically moved. The movements are controlled to introduce specific values of ϕ into the OPD.

6.7.2 Reconstruction algorithms

Equation (6.23) shows that there are three unknowns in the interferogram irradiance pattern: $I'(x,y)$, $I''(x,y)$ and $\Psi(x,y)$. The latter unknown is of primary interest since it encodes the OPD between the reference and test wavefronts. With three unknowns, at least three measurements with different values of ϕ are needed to recover $\Psi(x,y)$. A possible three-step algorithm has $\phi = \pi/3,\ \pi,$ and $5\pi/3$. In this case, three measurements are made such that

$$\begin{aligned}
&I\left(x,y;\frac{\pi}{3}\right) = I'(x,y) + I''(x,y)\cos\left[\frac{\pi}{3}\right]\cos[\Psi(x,y)] - I''(x,y)\sin\left[\frac{\pi}{3}\right]\sin[\Psi(x,y)],\\
&I(x,y;\pi) = I'(x,y) + I''(x,y)\cos[\pi]\cos[\Psi(x,y)] - I''(x,y)\sin[\pi]\sin[\Psi(x,y)],\\
&I\left(x,y;\frac{5\pi}{3}\right) = I'(x,y) + I''(x,y)\cos\left[\frac{5\pi}{3}\right]\cos[\Psi(x,y)] - I''(x,y)\sin\left[\frac{5\pi}{3}\right]\sin[\Psi(x,y)].
\end{aligned} \tag{6.24}$$

Reducing gives

$$\Psi(x,y) = \tan^{-1}\left[\sqrt{3}\frac{I(x,y;5\pi/3) - I(x,y;\pi/3)}{I(x,y;\,5\pi/3) + I(x,y;\,\pi/3) - 2I(x,y;\,\pi)}\right]. \tag{6.25}$$

Thus, the phase at each point (x,y) can be obtained from the irradiance values at the corresponding points in the three measurements. While the three-step algorithm gives an exact result, it is sensitive to errors in the value of ϕ and measurement noise. A wide variety of phase-shifting interferometry reconstruction algorithms have been proposed in an effort to reduce the noise sensitivity of the measurement. Four-step and five-step algorithms provide superior performance over the three-step algorithm.

In the four-step algorithm, $\phi = 0,\ \pi/2,\ \pi,$ and $3\pi/2$. The irradiance patterns of the four measurements are

$$\begin{aligned}
&I(x,y;0) = I'(x,y) + I''(x,y)\cos[\Psi(x,y)],\\
&I\left(x,y;\frac{\pi}{2}\right) = -I''(x,y)\sin[\Psi(x,y)],\\
&I(x,y;\pi) = I'(x,y) - I''(x,y)\cos[\Psi(x,y)],\\
&I\left(x,y;\frac{3\pi}{2}\right) = I''(x,y)\sin[\Psi(x,y)].
\end{aligned} \tag{6.26}$$

Solving for the phase gives

$$\Psi(x,y) = \tan^{-1}\left[\frac{I(x,y;3\pi/2) - I(x,y;\pi/2)}{I(x,y;0) - I(x,y;\pi)}\right]. \tag{6.27}$$

Finally, Schwider et al.[1] and later Hariharan et al.[2] describe a robust five-step algorithm. In this case, $\phi = 0$, $\pi/2$, π, $3\pi/2$, and 2π. Following a similar derivation as in the other algorithms, the phase for the five-step algorithm is

$$\Psi(x,y) = \tan^{-1}\left[\frac{2[I(x,y;\pi/2) - I(x,y;3\pi/2)]}{2I(x,y;\pi) - I(x,y;0) - I(x,y;2\pi)}\right]. \tag{6.28}$$

6.7.3 Phase unwrapping

Each of the algorithms used to recover $\Psi(x,y)$ leads to an expression involving the arctangent function. Arctangent has an inherent ambiguity, as multiples of 2π can be added to a given argument, and the arctangent will return the same result. The arctangent function has principal values in the range of $-\pi$ to π (noninclusive on the upper end) if the signs of the numerators and denominators in Eqs. (6.25), (6.27), and (6.28) are taken into account. If the phase function exceeds this range, the phase values will be wrapped back down into this range. A one-dimensional analysis is useful for illustrating the effects of phase wrapping. Suppose that the true phase has a spherical aberration profile as shown in Fig. 6.13(a). Reconstructing this phase pattern by applying the preceding algorithms to a series of phase-shifted interferograms leads to the profile shown in Fig. 6.13(b). In the center of the phase pattern, the original phase matches the wrapped phase. However, once the phase reaches a value of π in the periphery, the arctangent function wraps these values back into the range $-\pi$ to π by removing integer multiples of 2π from the actual value until the resultant value is within the range. The resultant wrapped wavefront has a series of discontinuous steps at the wrapping transitions.

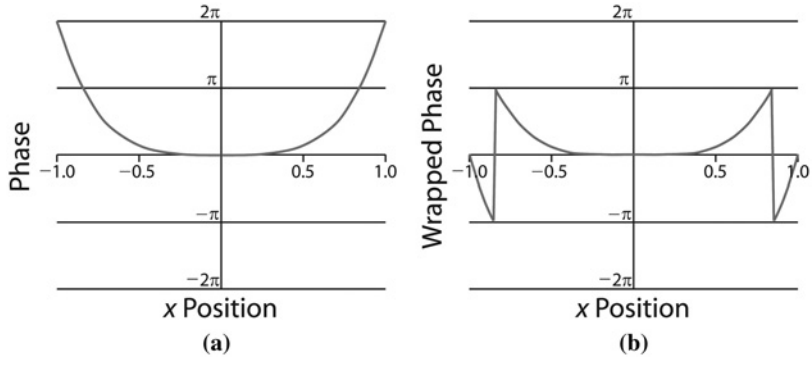

Figure 6.13 (a) Profile through a wavefront with spherical aberration. (b) Reconstruction of the wavefront leads to a phase-wrapped wavefront.

In general, the measured wavefront phase will exceed the range $-\pi$ to π, and its reconstruction will contain these wrapping artifacts. Examining Fig. 6.13, the wrapped phase contains the same information as the original phase. A value of 2π merely needs to be added to the peripheral region to recover the original phase pattern. While intuitive, algorithms for performing this phase unwrapping are sophisticated. See the book by Ghiglia and Pritt in the bibliography for a detailed discussion of the various phase-unwrapping algorithms. Here, a technique outlined by Peck[3] will be applied to the one-dimensional example above. Before proceeding, it is useful to define the wrapping operator, wrap( ), as

$$\text{wrap}(x) = [(x + \pi) \bmod 2\pi] - \pi. \tag{6.29}$$

Suppose that the original phase as shown in Fig. 6.13(a) is given by $\Psi(x_i)$, and the wrapped phase as shown in Fig. 6.13(b) is given by $\Phi(x_i) = \text{wrap}[\Psi(x_i)]$. The x_i are a series of discretely sampled points across the profile of the phase, with $i = 1 \ldots N$. A key observation in unwrapping the phase is that the slopes of both the original phase and the wrapped phase are identical except at the transition points. The next step in unwrapping the phase is to calculate the difference between the wrapped phase and its immediate neighbor such that $\Delta\Phi(x_i) = \Phi(x_{i+1}) - \Phi(x_i)$. This calculation is shown in Fig. 6.14(a). Two outlier points with values of approximately $\pm 2\pi$ appear at the wrapping points, while the remaining points are just the differences that would be expected in the original wavefront. The slope of the original wavefront can be approximated by

$$\text{slope}(x_i) \cong \frac{\text{wrap}[\Delta\Phi(x_i)]}{x_{i+1} - x_i}. \tag{6.30}$$

Equation (6.30) is essentially the finite-difference expression for the slope of the phase. The wrap( ) operator in the numerator, however, has the added effect of "filtering" out the outlier values that occur at the wrapping points

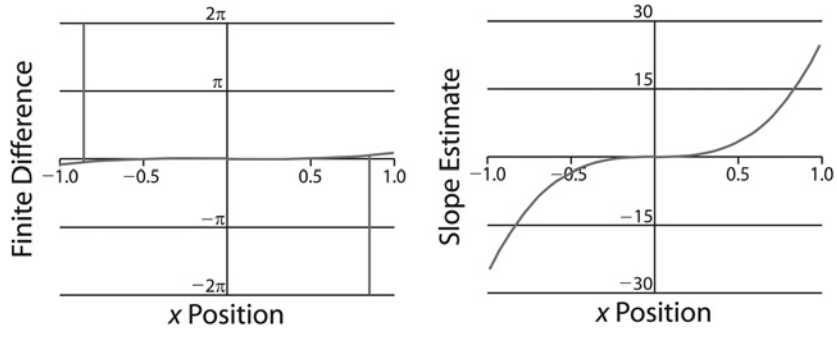

Figure 6.14 (a) Finite difference of the wrapped phase. (b) Estimate of the slope of the original wavefront.

and mapping them to something similar to the other slope values. The result of Eq. (6.30) is shown in Fig. 6.14(b). This slope estimate is then fit to a function and integrated to create an initial estimate of the original phase $\Psi_{est}(x_i)$.

The outlier values that were wrapped into the other difference values create some residual error in $\Psi_{est}(x_i)$. The residual errors can be calculated as

$$\text{residual error}(x_i) = \text{wrap}[\Phi(x_i) - \Psi_{est}(x_i)]. \tag{6.31}$$

The residual errors are shown in Fig. 6.15(a). Finally, a second estimate of the original wavefront $\tilde{\Psi}(x_i)$ is calculated as

$$\tilde{\Psi}(x_i) = \Psi_{est}(x_i) + \text{residual error}(x_i). \tag{6.32}$$

The resultant estimate of the original phase is shown in Fig. 6.15(b). In this noise-free example, the original phase is perfectly reconstructed by this process.

The preceding example is a one-dimensional application of the phase-unwrapping algorithm used to illustrate the steps of the algorithm. The process can be easily extended to two dimensions. Equation (6.30) is extended to calculate the slopes in both the x and y directions. The initial estimate of the original phase $\Psi_{est}(x_i, y_i)$ is obtained by fitting the slope data to the derivatives of the Zernike polynomials in the same manner as was done for the Shack–Hartmann reconstruction in Section 5.4.5. The coefficients of this fitting process are then used to reconstruct the initial estimate of the phase. Combining these results with the residual errors leads to the final estimate of the original phase.

6.8 Testing Aspheric Surfaces

Much of the preceding discussion on optical testing assumed spherical surfaces with small fabrication errors, or optical systems with small levels of aberration. In these cases, the interferograms created in the various testing

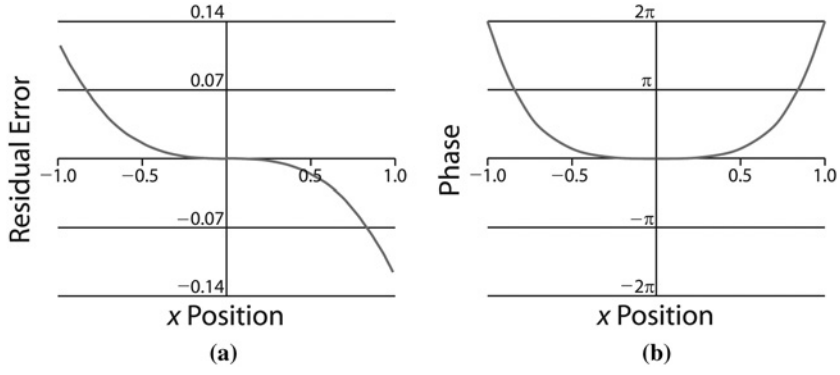

Figure 6.15 (a) Residual wrapped error. (b) Reconstructed phase.